AGU Advances

RESEARCH ARTICLE
10.1029/2021AV000520

Key Points:

- We report on the hafnium isotope, oxygen isotope and trace element compositions of 4.1–3.3 Ga detrital zircons from South Africa
- Pre-3.8 Ga zircons derived from long-lived crust with a mantle signature; post-3.8 Ga zircons show evidence for arc-like flux melting
- Other zircon suites show a similar transition in the 3.8–3.6 Ga time window, possibly indicating global onset of mobile-lid tectonics

Supporting Information:

Supporting Information may be found in the online version of this article.

Correspondence to:

N. Drabon,
ndrabon@fas.harvard.edu

Citation:

Drabon, N., Byerly, B. L., Byerly, G. R., Wooden, J. L., Wiedenbeck, M., Valley, J. W., et al. (2022). Destabilization of long-lived Hadean protocrust and the onset of pervasive hydrous melting at 3.8 Ga. *AGU Advances*, *3*, e2021AV000520. https://doi.org/10.1029/2021AV000520

Received 2 JUL 2021
Accepted 2 FEB 2022

Peer Review The peer review history for this article is available as a PDF in the Supporting Information.

Author Contributions:

Conceptualization: Nadja Drabon, Gary R. Byerly
Formal analysis: Michael Wiedenbeck, John W. Valley, Kouki Kitajima
Funding acquisition: Donald R. Lowe
Investigation: Nadja Drabon, Benjamin L. Byerly, Gary R. Byerly, Joseph L. Wooden
Methodology: Michael Wiedenbeck, John W. Valley, Kouki Kitajima

Destabilization of Long-Lived Hadean Protocrust and the Onset of Pervasive Hydrous Melting at 3.8 Ga

Nadja Drabon[1,2], Benjamin L. Byerly[3,4], Gary R. Byerly[5], Joseph L. Wooden[6], Michael Wiedenbeck[7], John W. Valley[8], Kouki Kitajima[8], Ann M. Bauer[8], and Donald R. Lowe[2]

[1]Department of Earth and Planetary Sciences, Harvard University, Cambridge, MA, USA, [2]Department of Geological Sciences, Stanford University, Stanford, CA, USA, [3]Department of Earth Sciences, University of California, Santa Barbara, CA, USA, [4]Now at Thermo Fisher Scientific, Waltham, MA, USA, [5]Department of Geology and Geophysics, Louisiana State University, Baton Rouge, LA, USA, [6]USGS Menlo Park and Stanford University, Stanford, CA, USA, [7]Helmholtz Centre Potsdam, GFZ German Research Centre for Geosciences, Potsdam, Germany, [8]Department of Geoscience, University of Wisconsin, Madison, WI, USA

Abstract The nature of Earth's earliest crust and crustal processes remain unresolved questions in Precambrian geology. While some hypotheses suggest that plate tectonics began in the Hadean, others suggest that the Hadean was characterized by long-lived protocrust and an absence of significant plate tectonic processes. Recently proposed trace-element proxies for the tectono-magmatic settings in which zircons formed are a relatively novel tool to understand crustal processes in the past. Here, we present high-spatial resolution zircon trace and rare earth element geochemical data along with Hf and O isotope data of a new location with Hadean materials, 4.1–3.3 Ga detrital zircons from the 3.31 Ga Green Sandstone Bed, Barberton Greenstone Belt. Together, the hafnium isotope and trace element geochemistry of the detrital zircons record a major transition in crustal processes. Zircons older than 3.8 Ga show evidence for isolated, long-lived protocrust derived by reworking of relatively undepleted mantle sources with limited remelting of surface-altered material. After 3.8 Ga, Hf isotopic evidence for this protocrust is muted while relatively juvenile source components for the zircon's parental magmas and flux-like melting signatures become more prominent. This shift mirrors changes in Hf isotopes and trace element geochemistry in other Archean terranes between ~3.8 and 3.6 Ga and supports the notion that the global onset of pervasive crustal instability and recycling—A possible sign for mobile-lid tectonics—Occurred in that time period.

Plain Language Summary The nature of Earth's earliest crust and crustal processes remains enigmatic due to the almost complete lack of a rock record older than 4.0 billion years (Ga, Hadean Eon) and the scarcity of rocks between 4.0 and 3.6 Ga (Eoarchean Era). One unresolved question is when mobile-lid tectonics commenced. To study the Hadean, the only direct record is from the mineral zircon, but Hadean zircon is rarely found. Here, we report a combination of isotopic and geochemical analyses on Hadean to Eoarchean zircons from the Barberton Greenstone Belt, South Africa, to expand our understanding of the changing nature of Earth's early crust. We find that pre-3.8 Ga zircons were not formed in a subduction zone setting, a hallmark of modern plate tectonics. Instead, the early crust originated from remelting of crust derived from a relatively undepleted mantle and, in comparison to modern mantle-derived crust, was distinctive in its longevity. Post- 3.8 Ga, geochemical signatures of the zircons start showing similarities to those of zircons derived from modern subduction zones. This shift can also be seen in other zircon suites in the 3.8–3.6 Ga time window, possibly indicating major transition in crustal geochemistry and global onset of mobile-lid tectonics in that time period.

1. Introduction

The nature of tectono-magmatic processes during early Earth history remains one of the major questions in Precambrian geology. Due to the lack of a rock record for Earth's first 500 Ma, this question is directly addressed primarily through the study of detrital zircon geochronology, isotope geochemistry, and trace and rare earth element (TREE) geochemistry. Certainly, the timing of the onset of mobile-lid tectonics has key implications for the evolution of early life. Today, mobile-lid tectonics is the major driver for volatile cycling and continental growth. Its onset would cause a substantial change in the compositions of the oceans and atmosphere, create new terrestrial habitats and, hence, play a key role in the evolution of life. From the limited evidence available, two

Supervision: Donald R. Lowe
Validation: Ann M. Bauer
Writing – original draft: Nadja Drabon
Writing – review & editing: Nadja Drabon, Benjamin L. Byerly, Gary R. Byerly, Joseph L. Wooden, Michael Wiedenbeck, John W. Valley, Ann M. Bauer, Donald R. Lowe

major hypotheses have emerged for crustal processes during the early Earth: Earth was more similar to today than previously thought and plate tectonics commenced shortly after Earth's formation (Hypothesis A), or the Hadean Earth was very different from today and was dominated by localized remelting of long-lived protocrust and an absence of significant plate tectonic activity (Hypothesis B). Hypothesis A is a uniformitarian model in which zircon-bearing Hadean rocks formed in plate-boundary settings (Harrison et al., 2018). In this scenario, active plate boundaries allowed for the recycling of mafic crust in subduction zones and transport of surface-derived volatiles into the mantle, causing flux melting. Hypothesis A is mainly based on unradiogenic Hf isotope values suggesting that significant silicate fractionation occurred (Bell et al., 2011, 2014; Harrison et al., 2005, 2008), zircon model melt compositions similar to modern arc rocks (Turner et al., 2020), low Ti-in-zircon temperatures suggestive of wet melting conditions (Harrison et al., 2018; Harrison & Schmitt, 2007; Watson & Harrison, 2005), and zircon mineral inclusions suggestive of broadly granitic (Maas et al., 1992; Peck et al., 2001) and perhaps even specifically peraluminous granitic protoliths (Bell et al., 2015; Harrison et al., 2018; Hopkins et al., 2008; Trail et al., 2017), although other researchers have proposed parent rocks similar to Archean tonalite, trondhjemite, granodiorite (TTGs) with more intermediate composition (Carley et al., 2018; Cavosie et al., 2005, 2019; Fu et al., 2008; Reimink et al., 2020). Hypothesis B is a non-uniformitarian model and is characterized by the absence of significant plate tectonic activity. In this regime, zircon-bearing rocks formed within long-lived protocrust, either in local oceanic plateaus or a global stagnant lid (e.g., Campbell & Griffiths, 1993; Kamber et al., 2003; Kemp et al., 2010; Shirey et al., 2008; Zeh et al., 2014). Hypothesis B is supported by whole rock Pb isotopic analyses from Greenland gneisses interpreted as Pb incorporated from a long-lived, 4.3 Ga basaltic source (Kamber et al., 2003) and Nuvvuagittuq TTGs interpreted to be derived from 4.3 to 4.4 Ga mafic protocrust based on Pb-Hf data (O'Neil et al., 2013). In addition, Hadean to Eoarchean zircons from different Archean terranes share subchondritic ε_{Hf} values that decrease through time along similar trajectories (Bauer et al., 2017; Bell et al., 2011; Chaudhuri et al., 2018; Kemp et al., 2010; Mueller & Wooden, 2012; Ranjan et al., 2020). This Hf pattern points to crustal processes dominated by in situ reworking of older crust rather than by reworking of relatively juvenile additions such as seen in modern plate margins. During the late Eoarchean between 3.8 and 3.6 Ga, these different Archean terranes show a shift to more radiogenic ε_{Hf} values indicating an influx of juvenile magmas (Bauer et al., 2017, 2020; Bell et al., 2014; Chaudhuri et al., 2018; Fisher & Vervoort, 2018; Mueller & Wooden, 2012), possibly signaling the global onset of mobile-lid tectonics (possibly sluggish plate tectonics) and more widespread continent formation (e.g., Fisher & Vervoort, 2018; Shirey et al., 2008; Vervoort et al., 2016, 2017).

To alleviate some of the uncertainty around the interpretation of the Hf isotope record of the Jack Hills zircons (e.g., Whitehouse et al., 2017), Turner et al. (2020) recently used zircon trace and rare earth element geochemistry (TREE) to calculate model melt compositions. They proposed that the Jack Hills zircons carried a subduction signature throughout the Hadean and Archean, at odds with non-uniformitarian models for the Hadean Earth. One problem with model melt compositions is the dependence of partition coefficients (Kds) on a range of parameters, including pressure, temperature, redox state and composition of the source (Blundy & Wood, 2003). In particular, temperature has a large effect on mineral-melt partitioning, and it is hence crucial to find Kds within the same temperature range, which may not always be available. Turner et al. (2020) used Kds applicable for high-temperature melts, yet all Jack Hills zircons yield relatively low Ti-in-zircon crystallization temperatures. The use of a specific set of Kds also introduces the problem that all zircons are treated as if they formed under a very limited range of conditions; however, due to the detrital nature of these zircons and the ∼1 Ga span of their ages, they must have been derived from multiple and/or evolving sources, each source likely requiring different Kds. The reliability of using detrital zircon TREEs to infer whole rock TREE compositions was recently called into question by a study comparing calculated model melt compositions of Eoarchean zircons from the Acasta Gneiss Complex with the whole rock composition; the zircon model melts did not match whole-rock REE patterns for any given set of zircon-melt Kds (Reimink et al., 2020).

Instead of calculating model melt compositions based on partition coefficients, a more robust approach is to directly evaluate zircon TREE. This way, the variation in relevant partitioning controls (i.e., source composition, pressure, temperature, and redox state) for each tectono-magmatic domain are accounted for and hence some of these uncertainties can be avoided. Based on a global compilation of several thousand igneous zircons, Grimes et al. (2015) have shown that several TREE ratios, especially those based on U-Th-Nb-Sc-Ce-Yb systematics, can discriminate between zircon from melts generated in modern subduction arc environments, those derived from melting of relatively depleted mantle sources such as mid-oceanic ridge environments, and those from relatively

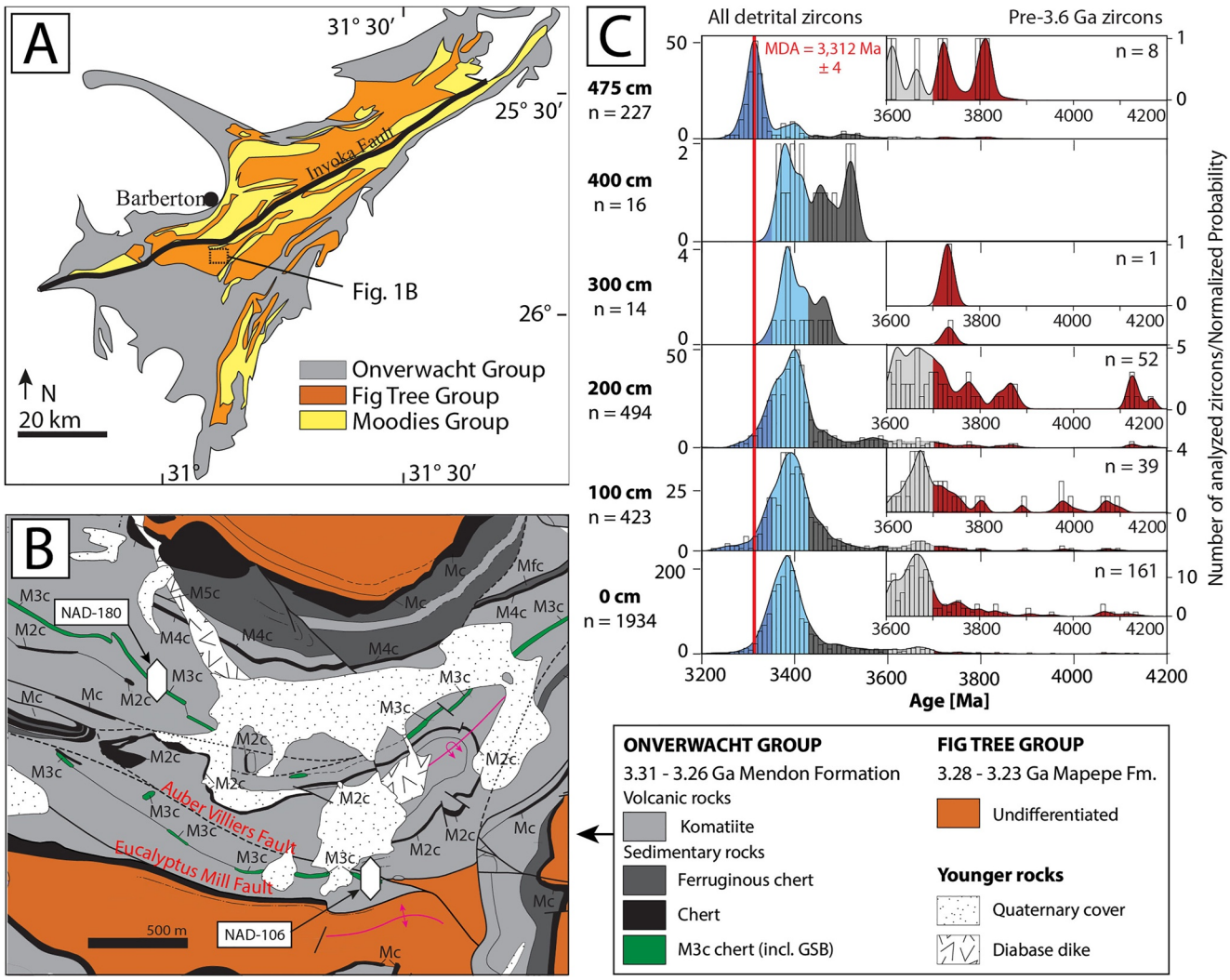

Figure 1. Map of the Barberton greenstone belt and detrital zircon geochronology of the Green Sandstones Bed (GSB). (a) Generalized map of the Barberton Greenstone Belt and (b) a detailed geological map of the study area modified from Lowe et al. (2012) with sample locations. Sample NAD-106 was taken from the GSB type locality and corresponds to sample numbers SA 22 and SA 51 of Byerly et al. (2018) Sample NAD-180 was taken from a second locality which corresponds to SA 811 of Byerly et al. (2018). (c) Probability density plots (PDPs) of $^{207}Pb/^{206}Pb$ detrital zircon geochronology from different stratigraphic intervals of the GSB. Insets represent detailed age spectra of zircons >3600 Ma. MDA = maximum depositional age. Colors of PDPs highlight different age clusters.

undepleted mantle sources such as plume-derived environments as seen in Iceland and Hawaii. These discriminatory ratios will remain diagnostic even if the crust experienced subsequent closed-system reworking within the same crustal setting. While the pioneering study by Grimes et al. (2015) requires follow-up to more broadly confirm these relationships and to explain the processes controlling them, additional studies are consistent with the Grimes et al. characterization (Barth et al., 2017, 2018; Coombs & Vazquez, 2014; Tang et al., 2017).

The Hadean to Paleoarchean crustal record is sparse, and the Jack Hills detrital zircon record often dominates the discussion of crust formation on the early Earth. A new location with relatively abundant Hadean zircons is the 3.31 Ga Green Sandstone Bed (GSB), South Africa, which has undergone lower grade metamorphism than all other known Hadean detrital zircon localities (Byerly et al., 2018; Drabon et al., 2021; R. R. Fu et al., 2021). The GSB zircons provide a unique record of the early Earth to test the robustness of crustal evolution models. The GSB shows excellent preservation because the sediment was silicified prior to compaction and subsequently experienced only lower greenschist-grade metamorphism (Tice et al., 2004). Overall, the zircons of the GSB record ~800 My of silicic igneous activity from 4.15 to 3.31 Ga (Figure 1, Figure S1 in Supporting Information S1), with major age clusters at 3.31 Ga (at the top of the GSB), 3.38 Ga (at the base of the GSB), and

minor clusters at 3.65 Ga and 4.1 Ga (Byerly et al., 2018; Drabon et al., 2021). Lowe et al. (2021) studied the sedimentology, stratigraphy, and provenance of the GSB. They found that the sources to the GSB may have been uplifted by the S6 meteorite impact far removed from the present-day BGB and that the sediments were transported for long distances to the site of deposition by aeolian processes. R. R. Fu et al. (2021) studied the paleomagnetic record of 19 zircons >3.5 Ga in the GSB but found that GSB zircons have magnetic moments nearly one order of magnitude weaker than Jack Hills zircons, precluding the retention of primary paleomagnetic information. Most relevant to this study, Drabon et al. (2021) have shown that the trace element signature of the Hadean zircons of the GSB are primary and consistent with a relatively undepleted mantle source, such as seen in Iceland or Hawaii. The zircons were derived from magma compositions ranging from higher temperature, more primitive magmas to lower temperature, more evolved TTG-like magmas that experienced some reworking of hydrated crust. However, the long-term evolution of crustal sources from the Hadean to the Mesoarchean in the source region is still unresolved. Here, we use the TREE signatures combined with Hf and O isotope ratios of the excellently preserved GSB zircons to characterize the crustal processes active in the source. Furthermore, we reevaluate the trace element signatures of zircons from the Jack Hills to test the robustness of a possible global crustal transition in the 3.8 to 3.6 Ga time window.

2. Materials and Methods

Zircons used for this study were previously dated by Drabon et al. (2021) (Data Sets S1 and S2 in Supporting Information S1; for methodology see original manuscripts) and Byerly et al. (2018) and were obtained from the GSB type locality (NAD-106; S25°54'33.11" and E31° 2'42.35") and a second locality further west (NAD-180; S25°53'56.50" and E31° 2'2.13"; Figure 1b). We analyzed these zircons for their Lu-Hf isotope (Data Sets S3–S5 in Supporting Information S1), TREE geochemical (Data Set S6 in Supporting Information S1), and O isotope compositions (Data Set S7 in Supporting Information S1). Where zircons were large enough, multiple analyses were performed on a single grain. The relatively small size of the zircons (generally <100 μm) and the necessary order of analyses (e.g., U-Pb first) required that often only a sub-selection of geochemical criteria could be coupled within the same zircons.

2.1. Hafnium Isotope Analyses

Lu-Hf isotope analyses were conducted on 329 zircons during two analytical sessions at the Arizona LaserChron Laboratory. Lu-Hf isotope laser ablation analyses had a beam diameter of 40 μm and were placed directly on top of the LA-ICP-MS U-Pb analysis pit (Figure S2 in Supporting Information S1). Cathodoluminescence (CL) images of the zircons were subsequently evaluated to only include analyses in which the Hf and U-Pb spots were within the same domain. We monitored isotopic and interelement ratios during sequential U-Pb and Hf isotope measurements to ensure that the ablations did not pass through more than one zircon domain. Due to the small size of the zircons, we were not able to perform multiple analyses on a single grain. Six zircon reference materials were used: 91,500, Mud Tank, Temora, Plešovice, FC1, and R33 (see Figure S3 in Supporting Information S1 for $^{176}Hf/^{177}Hf$ and $^{176}Lu/^{177}Hf$ of 91,500, see Data Set S4 in Supporting Information S1 for plot of all other reference materials). We followed the methods described in (Gehrels & Pecha, 2014) and (Ibanez-Mejia et al., 2014). Zircons were ablated using a Photon Machines Analyte G2 excimer laser system. Typical Hf signals were ~2–5 V of ^{180}Hf. Unknowns were run in blocks of 25 bracketed by measurements of reference zircons 91,500, R33, Mud Tank, Temora-2, Plesovice, and FC-53. Zircon Lu-Hf isotopic data were reduced line-by-line using "HfCalc," the LaserChron in-house data reduction program. Initial epsilon (ε) Hf values were calculated using the present-day Lu–Hf CHUR values of Bouvier et al. (2008) and the $\lambda(^{176}Lu)$ of Scherer et al. (2001) and Söderlund et al. (2004). All Hf isotopic data are reported as ε_{HfT}, evaluated at the time of crystallization based on the $^{206}Pb/^{207}Pb$ age. Reported uncertainties for $^{176}Hf/^{177}Hf$ reflect the in-run uncertainty, and the reported 2se in ε_{HfT} units do not account for age or $^{176}Lu/^{177}Hf$ uncertainty and therefore represent minimum uncertainties. However, the $^{176}Lu/^{177}Hf$ uncertainties are (conservatively) <3% (2se) and uncertainties of this magnitude would not contribute significantly to the ε_{HfT}. Data reduction and reporting protocols follow the recommendations of Fisher et al. (2014). Hf isotope ratio uncertainties are reported as the standard error (SE) of the mean at the 95% confidence interval. For the zircon reference materials, the $^{176}Hf/^{177}Hf$ 2SD reproducibility ranges from 0.000054 to 0.000084 (session 1) and 0.000012 to 0.000067 (session 2), with averages of 0.000070 and 0.000049, respectively (Data Set S4 in Supporting Information S1). The within-session deviation between measured and true

reference material $^{176}Hf/^{177}Hf$ ranges from 0.000001 to 0.000048. For detrital zircon analyses, it is impossible to evaluate a population and therefore a conservative estimate of the uncertainty is the reproducibility of the reference material analyses (Fisher et al., 2014), which for our data set is sometimes larger than the SE of the unknowns. The average reproducibility of the zircon reference materials is indicated with symbols in Figure 2. LA-ICP-MS ages were used to calculate initial ε values with the exception of two zircons. These include one grain where cracks probably affected the LA-ICP-MS analysis but not the SHRIMP U-Pb analysis (SA811p2-158) and one grain where multiple SHRIMP analyses consistently yield ages ∼100 Ma older than the LA-ICP-MS analysis (SA811p2-163). We use the same depleted mantle array starting at 3.8 Ga as suggested by Vervoort et al. (2017). The zircon reference material and sample results between the two sessions agree well (Figures S3 and S4; Data-Sets S4 and S5 in Supporting Information S1).

2.2. Trace and Rare Earth Element Analyses

Zircon trace element analyses were conducted on the SHRIMP-RG (reverse geometry) ion microprobe in the co-operated Stanford and U. S. Geological Survey SUMAC facility at Stanford University (SU), using the same techniques and instrument as in Grimes et al. (2015). Prior to analysis, the LA-ICP-MS holes on the zircons were filled with superglue and lightly repolished to make them flat to minimize topography. The mounts were then cleaned with a 10% ethylenediaminetetraacetic acid, thoroughly rinsed with DI water, and dried at 50°C in a vacuum oven for 30 min. The sample surface was coated with ∼10–20 nm of gold for conductivity and immediately loaded into the instrument sample lock chamber for storage at high vacuum ($<10^{-7}$ torr) to minimize outgassing during analysis.

An O_2^- primary beam with accelerating voltage of 10 kV was used to sputter secondary ions from the sample surface with a 0.8–2.8 nA primary beam current focused to ∼15–20 µm. Prior to analysis, spots were pre-sputtered for 60 s using a ∼40 µm raster to remove gold coating and surface contamination, and the primary and secondary beams were auto-tuned to maximize transmission. The acquisition included analysis of 37 masses: $^{7}Li^+$, $^{11}B^+$, $^{19}F^+$ (sessions 2,3), $^{23}Na^+$, $^{27}Al^+$, $^{30}Si^+$, $^{31}P^+$, $^{39}K^+$, $^{40}Ca^+$, $^{28}Si^{16}O^+$ (sessions 2,3), $^{45}Sc^+$, $^{30}Si^{16}O$ (session 1), $^{48}Ti^+$ (sessions 2,3), $^{49}Ti^+$, $^{56}Fe^+$, $^{89}Y^+$, $^{93}Nb^+$, $^{92}Zr^1H^+$, $^{96}Zr^+$, $^{139}La^+$, $^{140}Ce^+$, $^{146}Nd^+$, $^{147}Sm^+$, $^{153}Eu^+$, $^{155}Gd^+$, $^{165}Ho^+$, $^{159}Tb^{16}O^+$, $^{162}Dy^{16}O^+$, $^{166}Er^{16}O^+$, $^{169}Tm^{16}O^+$ (sessions 2,3), $^{172}Yb^{16}O^+$, $^{175}Lu^{16}O^+$, $^{90}Zr_2{}^{16}O^+$, $^{180}Hf^{16}O^+$, $^{206}Pb^+$, $^{207}Pb^+$, $^{232}Th^{16}O$, and $^{238}U^{16}O^+$. Count times ranged from 2 to 15 s per mass to optimize counting statistics for each isotope. Data were collected over 1 scan per spot for a total run time of ∼18 min, collected by magnet peak-jumping on an ETP discrete-dynode electron multiplier. The background for the electron multiplier is very low (<0.05 cps) and is statistically insignificant for the trace elements reported in this study.

The SHRIMP-RG was designed to provide higher mass resolution than other forward geometry large-format ion microprobe instruments (Clement & Compston, 1994), and can operate at high mass resolution without an energy filter with minimal loss of transmission of secondary ions. The mass resolution (M/ΔM) was set to ∼12,000 (measured on ^{89}Y) to resolve interfering molecular species, particularly for ^{45}Sc, ^{48}Ti, and REE. ^{93}Nb requires mass resolution of ∼14,325 (10% peak height) to fully resolve it from $^{92}Zr^1H$, and is therefore measured on the shoulder of the peak-flat to avoid the overlapping interference.

Trace element concentration data were standardized against the well-characterized MAD-559 zircon material (Coble et al., 2018) and 91,500 (Wiedenbeck et al., 2004) was analyzed as a secondary reference material. Data were reduced using the MS Excel add-in program Squid2.51 from Ken Ludwig (2001), following procedures reported by Grimes et al. (2015). All inter-element ratios were normalized to ^{30}Si during our first session and $^{28}Si^{16}O^+$ on sessions 2 and 3. A small number of individual analyses were not recorded because a sudden fluctuation in signal indicated that the ratios may not be reliable for that analysis. All TREE data are reported in the Data Set S6 in Supporting Information S1.

2.3. Oxygen Isotope Analyses

Oxygen isotope analyses were conducted at the WiscSIMS National Facility for Stable Isotope Geochemistry at the University of Wisconsin-Madison, USA, and the GeoForschungsZentrum (GFZ) in Potsdam, Germany. In total, we conducted 277 analyses. Overall, the analytical results of the two O isotope sessions agree well, confirming that little to no bias exist between the two facilities (Figure S5a in Supporting Information S1). Thirty-eight zircons were analyzed with two spots and seven were analyzed with three spots. When multiple spots

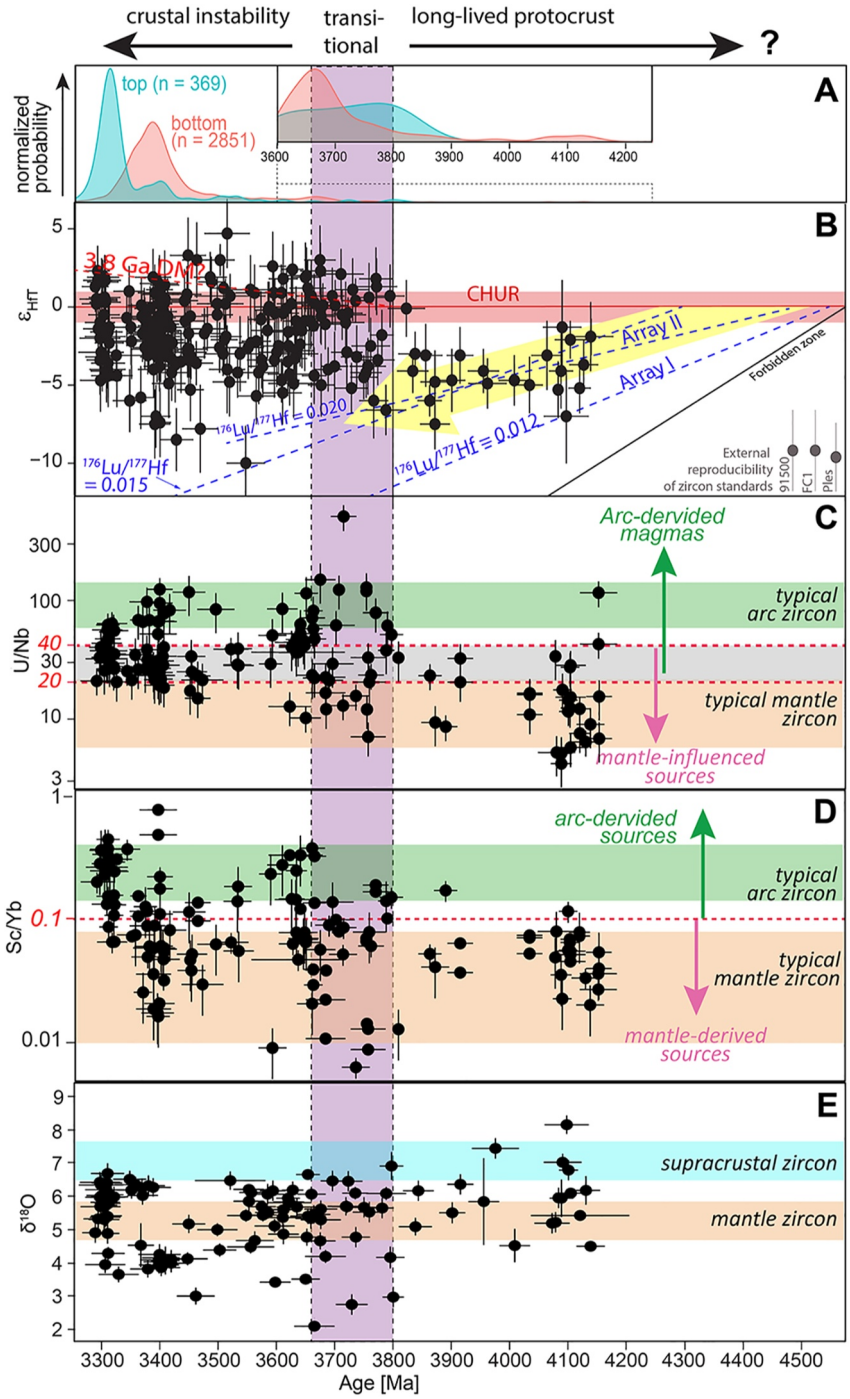

Figure 2. Compilation of zircon isotope and trace element results. (a) Probability density functions of detrital zircons from the base (0–200 cm stratigraphic height) and top (475 cm) of the Green Sandstone Bed. Inset is detailed enlargement of the older zircon populations. (b) $\varepsilon_{Hf(T)}$ versus time. The inset shows long-term 2SD for three of the analyzed reference materials (91,500, FC-1, and Plesovice). (c) U/Nb versus time. Zircons derived from magmatic arcs have values of U/Nb ≥ 20 and those from mantle-derived melts of U/Nb ≤ 40 (Grimes et al., 2015). Gray bar reflects the zone in which arc and mantle signatures overlap. The green bar indicates first to third quartile of typical Phanerozoic continental arcs. The orange bar indicates first to third quartile of typical Phanerozoic depleted and relatively undepleted mantle sources (MORB and ocean islands). (d) Sc/Yb versus time. Grimes et al. (2015) determined Sc/Yb of 0.1 as a demarcation value between arc- and mantle-related settings (red dashed line), though some overlap exists (see Figure 3c). The green bar indicates first to third quartile of typical Phanerozoic continental arcs. The orange bar indicates first to third quartile of typical Phanerozoic depleted and relatively undepleted mantle sources (MORB and ocean islands). (e) $\delta^{18}O$ versus time. All data presented here are from filtered zircons only (see methods for filtering criteria). DM = depleted mantle. All uncertainties are plotted as 2s.

were analyzed within a single zircon, most zircons showed good reproducibility (0.24 ‰ difference on average for analyses that passed all filters). Only two of these grains show deviation in their $\delta^{18}O$ values, indicating differential zircon response to secondary alteration (Figure S5b in Supporting Information S1).

At WiscSIMS, $\delta^{18}O$ and $^{16}OH/^{16}O$ data were obtained over two days using the CAMECA IMS-1280 ion microprobe. Analyses were done in multicollector mode, analyzing $^{16}O^-$, $^{18}O^-$ and $^{16}O^1H^-$, by following procedures described elsewhere (Kita et al., 2009; Valley & Kita, 2009; Wang et al., 2014). The zircons were compared to the reference zircon KIM-5 ($\delta^{18}O = 5.09‰$ VSMOW; Valley, 2003). A $^{133}Cs^+$ primary ion beam with a total impact energy of 20 keV was focused on the sample surface for 3.5 min (incl. 10 s of pre-sputtering, 120 s of automatic tuning of the secondary beam, and 80s of data acquisition). The spot size was 8 × 9 μm at the sample surface. The spot-to-spot precision of individual $\delta^{18}O$ analyses is estimated to be the two standard deviations (2s) of the reproducibility of bracketing zircon reference material KIM-5 (on average 0.24‰), as discussed previously (Kita et al., 2009; Valley & Kita, 2009). WiscSIMS oxygen isotope data are reported in the Data Set S7 in Supporting Information S1.

At the GFZ, a Cameca 1280-HR was used to analyze zircon during a single session that lasted over a four-day period. Machine calibration was based on the zircon reference material 91,500 ($\delta^{18}O = 9.86$ ‰; Wiedenbeck et al., 2004) and the quality control material Temora2 ($\delta^{18}O = 8.20$ ‰; Valley, 2003). The SIMS analyses employed a $^{133}Cs+$ primary beam with a total impact energy of 20 keV and were run in static multi-collection mode. The primary ion beam was focused to a ca. 6 or 3 μm diameter depending on the primary ion current used for a given analysis. Each analysis was preceded by an 80 s pre-sputtering using either a 20 or a 15 μm raster, needed to locally remove the gold coat and to establish equilibrium sputtering conditions. The primary beam was rastered over an area of between 15 × 15 μm, 8 × 8 μm, and 5 × 5 μm during data acquisition, the size depending on the amount of space available on the given zircon grain. Each change in primary raster parameters was accompanied by its own individual calibration using that raster on both the primary reference material (91,500) and the quality control material (Temora2). Ongoing checks of the reference material 91,500 found no detectable drift in instrumental mass fractionation during our session and the repeatability of the 91,500 reference material was ±0.30‰ (2s), or better, regardless of the primary beam current that was employed. For Temora2, a slight bias was detected ranging from 0.07 to 0.22‰ toward a lighter isotope ratio as compared to the recommended value. Based on these observations, the data are reliable at the ±0.4‰ level (2s) or better when considering both bias and repeatability. GeoForschungsZentrum oxygen isotope data are reported in the Data Set S7 in Supporting Information S1.

2.4. Filtering of Hf, O, and TREE Data

The isotopic and geochemical measurements can be biased by chemical alteration, especially in radiation-damaged zones, cracks, or inclusions. The SIMS and laser beams were focused on sites with no obvious impurities and imaged with CL, back scattered electron and/or transmitted light microscopy after analyses to identify analysis spots that were located on subsurface cracks or inclusions (Figure S2; Data Sets S8 and S9 in Supporting Information S1). A few grains were lost due to subsequent cleaning and could not be imaged. We excluded all analyses where the analytical pits revealed such cracks or inclusions. Furthermore, we used zircon CL textures to differentiate igneous from metamorphic zircon and to ensure that the analyses were conducted in the same crystallographic domain as the U-Pb analyses (Cavosie et al., 2005; Hoskin & Black, 2000). Of the CL-imaged zircons, oscillatory zonation is most common ($n = 247$), indicating that the majority of the zircons are of igneous origin. Other well-known igneous zonation patterns, such as sector zoning ($n = 14$), do occur but are relatively rare. A few zircons show complex patterns ($n = 10$). Indicators of zircon alteration, such as homogenous ($n = 53$) or patchy ($n = 31$) CL patterns are relatively more common in the older zircons. Otherwise, no obvious trend between zonation type and age of the zircons was observed. We rejected analyses that were located on rims, that mixed domains (i.e., mix of core and rim), or from zircons with CL patterns that were not obviously igneous. For hafnium isotope analyses at the LaserChron Lab, all analyses were screened for within-sample zonation in $^{176}Hf/^{177}Hf$ and $^{176}Lu/^{177}Hf$. Zircons in which ablation revealed the transition between two or more domains with distinctly different initial $^{176}Hf/^{177}Hf$ (variation outside of ~0.000070 2se, which is near the upper bound of uncertainties in this study) during a single analysis, and analyses that burned through the zircon were excluded. For oxygen isotope analyses at WiscSIMS, $^{16}OH/^{16}O$ is an effective parameter to monitor alteration of radiation-damaged domains in zircon that have been altered (Wang et al., 2014). We excluded analyzed zircons

with elevated background-corrected $^{16}OH/^{16}O$ ($>7 \times 10^{-4}$) as they are hydrous and likely appreciably radiation-damaged (Figure S6a in Supporting Information S1). We furthermore filtered zircons with high internal 2s uncertainties (>0.36‰, Figure S6b in Supporting Information S1) and low yields (<1.67 Gcps/nA, Figure S6c in Supporting Information S1). For $\delta^{18}O$ analyses at the GFZ, zircons with low ^{16}O counts per second ($<2.1 \times 10^9$ at 15 μm beam, Figure S7 in Supporting Information S1) were discarded. For TREE analyses, we applied conservative geochemical screens to filter analyses that show elemental enrichments of non-constituent cations and thus signify contamination or alteration related to metamictization (Grimes et al., 2015), resulting in the exclusion of about a third of the analyses. Ca and P serve as screens for apatite inclusions and we excluded zircons with high Ca (>50 ppm) and high P abundances (>1,000 pm). Similarly, cracks commonly contain iron and titanium oxides (Harrison & Schmitt, 2007) and thus we excluded analyses with elevated Fe (>100 ppm). Grains with high Al abundance (>100 ppm) were excluded as well as they signify glassy or feldspathic melt inclusions, or altered (i.e., metamict) domains. Analyses that passed all filters are combined in Data Set S10 in Supporting Information S1.

3. Results

3.1. Hf Isotope Results

Hf isotope compositions for the 4.15–3.80 Ga GSB zircons are subchondritic, ranging from a maximum value of −1 $\varepsilon_{Hf(T)}$ units at 4.1 Ga to values as low as −7.5 $\varepsilon_{Hf(T)}$ units at 3.8 Ga. The majority of these data fall on a broad crustal $\varepsilon_{Hf(T)}$ versus age array with increasingly negative $\varepsilon_{Hf(T)}$ values persisting until shortly after 3.8 Ga (Figure 2b). At least one Hadean zircon (SA811p2-186, 4097 ± 19 Ma, 92% concordance) falls significantly below this main $\varepsilon_{Hf(T)}$-time array and exhibits an $\varepsilon_{Hf(T)}$ value of −7.0 ± 3 (2s, Figure 2b). Because this zircon shows oscillatory zoning in cathodoluminescence (CL; Figure S2 in Supporting Information S1), Th/U values >0.1 and consistency between three $\delta^{18}O_{VSMOW}$ spots (8.03 ± 0.27 ‰, 8.06 ± 0.27 ‰, and 8.28 ± 0.27 ‰; 2s, Data Set S7 in Supporting Information S1), we interpret the $\varepsilon_{Hf(T)}$ value to be primary. It is notable that no zircons older than 3.8 Ga have superchronditic $\varepsilon_{Hf(T)}$ values.

Starting at 3.8 Ga, the $\varepsilon_{Hf(T)}$ values become more varied (generally between −6 and +3), including a significant number of chondritic and superchondritic values (Figure 2b). The occurrence of values at or above CHUR suggests that zircon was being derived from juvenile magmatic additions to the crust. At the same time, the presence of values below CHUR supports mixing with and/or reworking of older crust. It is notable that the main Hadean $\varepsilon_{Hf(T)}$-time array attenuates shortly after 3.8 Ga. Only a single post-3.8 Ga $\varepsilon_{Hf(T)}$ analysis (SA51p1-287) at 3548 ± 16 Ma (98% concordance) with faint oscillatory CL pattern, Th/U of 0.82 (U = 362 ppm; Th = 297 ppm), and a mantle-like $\delta^{18}O$ value (5.44 ± 0.18‰, 2s) fits that array.

After 3.43 Ga, the data plot along vertical age-$\varepsilon_{Hf(T)}$ trends (Figure 2b). The dominant zircon-age cluster of the GSB at 3.38 Ga shows predominantly subchondritic $\varepsilon_{Hf(T)}$ values with a range in values extending between −8 and +2. The age cluster at 3.31 Ga shows a spread in values from slightly subchondritic (−1 to −6 $\varepsilon_{Hf(T)}$ units) at the base of the GSB to slightly superchondritic (3 to −2 s_{haft} units; Figure S4a in Supporting Information S1) at the top, indicative of a shift in magma composition during a single magmatic episode.

3.2. Trace Element Geochemistry and Petrogenetic Implications

The vast majority of zircons in the GSB show TREE signatures similar to pristine igneous zircon. Metamorphic zircons typically display a Th/U < 0.1 (Hoskin & Black, 2000), whereas GSB zircons have Th/U values well above 0.1 (only two zircons that passed all other filters have <0.1; see methods for description of filters). Similarly, the GSB zircons show chondrite-normalized REE patterns with light REE depletion, heavy REE enrichment, a positive Ce anomaly, and a negative Eu anomaly (Figure S8 in Supporting Information S1) which are consistent with an igneous origin and compositions unaffected by alteration associated with metamictization (Hoskin & Schaltegger, 2003).

To distinguish arc from non-arc zircon sources, ratios of U-Nb-Sc-Ce-Yb are especially reliable when several discriminatory element ratios are considered together (Barth et al., 2017; Grimes et al., 2015; Figures 2 and 3; Figure S9 in Supporting Information S1 for discrimination diagrams using U/Nb, Nb/Sc, Ce/Nb, Sc/Yb, and Sc/U) because local petrogenetic processes may affect individual trace element ratios but are unlikely to affect all proxies collectively. Furthermore, Drabon et al. (2021) have shown that secular cooling did not significantly affect

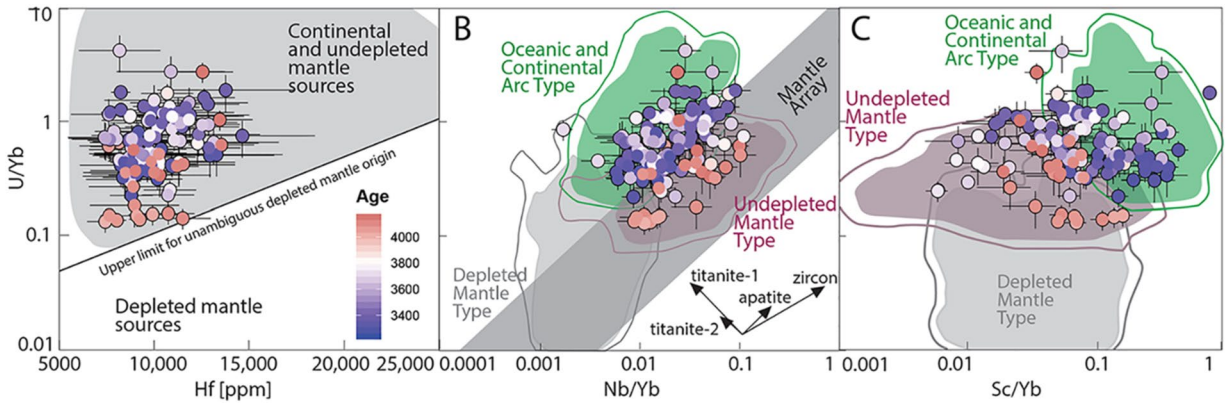

Figure 3. Trace and rare earth element plots after Grimes et al. (2015). (a) U/Yb ratio versus Hf for zircons from the Green Sandstone Bed. (b) U/Yb versus Nb/Yb with insets showing the effect of open-system (Rayleigh) fractionation of select minerals on the displayed system (Grimes et al., 2015). The upper boundary of the zircon mantle array roughly represents a U/Nb of ~20. (c) U/Yb versus Sc/Yb. Colored fields represent a global compilation of zircons from different Phanerozoic tectono-magmatic settings (Grimes et al., 2015). The outer contour line is shown at the 95% level which represent the proportion of the distribution within the contour. See Figure S9 in Supporting Information S1 for additional discrimination diagrams using U/Nb, Nb/Sc, Ce/Nb, Sc/Yb, and Sc/U). All uncertainties plotted as 2s.

these crucial trace element ratios and that the tectono-magmatic fields in the Grimes discrimination diagrams are still applicable for Paleoarchean to Hadean zircons. The most reliable proxies used for identifying those zircon that formed in a subduction-zone environment discussed here are (1) the relative depletion of Nb (i.e., higher U/Nb values; Figures 2c and 3b) and (2) the relative enrichment of Sc (i.e., higher Sc/Yb values; Figures 2d and 3c):

(1) The relationship between U and Nb in magmatic systems is influenced by depth of melting, metamorphic dehydration of oceanic crust (Baier et al., 2008; Pearce, 1982), variations in mantle source composition (as is seen today between modern mid-oceanic ridge and plume magmas) and crustal assimilation (Grimes et al., 2015). In U/Yb versus Nb/Yb space (Figure 3b), mantle-derived zircons define an empirically determined mantle array with the upper boundary roughly representing a U/Nb value of 20. Within this mantle array, zircon derived from depleted mantle melts can generally be distinguished from those derived from relatively undepleted mantle melts (and arc magmas) by lower Nb/Yb (<0.005) and lower U/Yb values (<0.1; Figure 3b). Zircon from subduction settings, on the other hand, can be distinguished from zircon from mantle-derived settings by the relative depletion in Nb and enrichment of U. This is displayed by a shift toward lower or buffered Nb/Yb values and increasing U/Yb values (i.e., an increase in U/Nb values) compared to typical mantle compositions (Figure 3b). In U/Yb versus Nb/Yb space, there is some overlap between the arc and mantle fields, with zircon derived from magmatic arcs having U/Nb values >20 while those derived from depleted and relatively undepleted mantle generally display values <40 (Figures 2c and 3b). Lastly, it should be noted that Nb depletion does not provide conclusive evidence for subduction processes as these signatures could perhaps be formed by alternative mobile-lid tectonic processes that caused burial of hydrated crust, such as through sagduction/partial convective overturn.

Most pre-3.8 Ga zircons fall into the relatively undepleted mantle field (Figures 2c and 3b). Most U/Nb values (average 17.6) are far lower than the typical range of magmatic-arc signatures in modern zircons (typically U/Nb of 56–131, Figure 2c) and are more like those in relatively undepleted mantle sources such as seen today in Iceland or Hawaii (U/Nb of 13–19; Grimes et al., 2015). These results confirm those from Drabon et al. (2021) for Hadean GSB zircons and extend the predominance of the undepleted mantle signature to 3.8 Ga. Only a single pre-3.8 Ga zircon plots above the mantle array toward higher U/Yb and relatively lower Nb/Yb values (i.e., U/Nb > 40; Figure 3b), a signal that at least some crust may have experienced subduction-like flux melting of basalt. From 3.80 to 3.65 Ga, the zircons show a spread in compositions, ranging from U/Nb of 7–151 (average 67.7 with one outlier at 525; Figure 2c), with roughly equal numbers falling into the fields for both arc and mantle sources. After 3.65 Ga, U/Nb values are generally but not exclusively >20 (average 42.6); many of the zircons plot in the arc field or within the transitional zone between mantle and arc fields, and could thus represent either process.

(2) Scandium enrichment, as tracked by Sc/Yb in zircon (Figures 2d and 3c), is also a reliable proxy for distinguishing melts produced in a subduction zone vs. melting of relatively depleted and undepleted mantle sources (Grimes et al., 2015). Grimes et al. (2015) suggest that Sc concentrations are low in zircons associated with melts derived by non-arc melting of mantle sources (i.e., melting of the relatively undepleted or depleted mantle)

because these environments produce almost exclusively basaltic melt that must undergo extensive fractionation to produce a sufficiently silica-rich melt that will be saturated in zircon. During this extensive fractionation, the residual melt is depleted in Sc by fractionation of the ferromagnesian minerals, clinopyroxene and amphibole. Primary melts produced in modern arc environments are more silicic in character and, depending on the starting Zr concentration, can either directly saturate in zircon or can saturate with much less fractionation. As a consequence, Sc/Yb values are relatively elevated for zircons in arc environments (roughly >0.1; Figures 2d and 3c; Grimes et al., 2015). In contrast, depleted or relatively undepleted mantle magmas require extensive fractionation before zircon can crystallize, resulting in low Sc and low Sc/Yb values (Figures 2d and 3c; Grimes et al., 2015).

In U/Yb versus Sc/Yb space, GSB zircons older than 3.8 Ga fall predominantly within the relatively undepleted mantle field (Figures 2d and 3c; Drabon et al., 2021). These zircons show Sc (average 17.4 ppm) and Sc/Yb (average 0.06) values lower than what is typical for zircons from modern continental arcs (Sc from 48 to 147 ppm; generally Sc/Yb > 0.1) and are in agreement with predominantly undepleted and depleted mantle melting signatures (Sc from 5 to 30 ppm; generally Sc/Yb < 0.1; Grimes et al., 2015; Figures 2d and 3c). After 3.8 Ga, zircons fall both into the relatively undepleted mantle and arc fields. Elevated Sc/Yb values become more common and high-Sc/Yb clusters at 3.65 and 3.31 Ga show distinct arc-like magmatic signatures (Figures 2d and 3c).

In summary, the U-Nb-Sc-Ce-Yb proxies collectively (Figures 2 and 3; Figure S9 in Supporting Information S1) reveal geochemical signatures in zircons older than 3.8 Ga that fall into the field of relatively undepleted mantle, similar in composition to modern zircons from Iceland or Hawaii, with only minor overlap with the field for arc-like melting signatures. After 3.8 Ga, the trace element proxies collectively reveal roughly equal numbers of zircons with signatures similar to modern arcs and undepleted mantle environments.

3.3. Oxygen Isotope Results

Oxygen isotope ratios in zircon are temperature-dependent tracers of fluid and solid interactions in the crust (Cavosie et al., 2009; Valley et al., 1998, 2005). Zircons with $\delta^{18}O_{VSMOW}$ values of 5.3 ± 0.6 ‰ (2s) are consistent with melts derived from the mantle (Cavosie et al., 2009; Valley et al., 1998, 2005); there is no evidence for significant secular variations in the $\delta^{18}O$ values of the mantle from the Hadean to today (Valley et al., 2005). The value for mantle zircon was defined with high accuracy and high precision (±0.1‰, 2s) laser fluorination analyses for ~2 mg sample splits of zircon. SIMS analyses have sample sizes a million times smaller than conventional determination though nonetheless providing a typical 2s precision of ±0.3 ‰ (2s) or better. Hence, SIMS $\delta^{18}O$ data that are only 0.2 ‰ above or below the "mantle-like" field cannot be confidently excluded from that field (i.e., 5.3 ± 0.8 vs. 5.3 ± 0.6). Zircons that crystallized in melts that formed from or assimilated crust altered at low temperature can show higher values (>6.5 ‰) and zircons that assimilated crust altered by surface waters at high temperature can show lower values than the mantle (Valley et al., 2005).

Of the pre-3.8 Ga zircons from the GSB, nine grains have values either within or slightly above but within 2s uncertainty of the mantle field (Figure 2e, Data Set S6 in Supporting Information S1). Seven zircons fall above the mantle field, four of which fall clearly within the supracrustal field (i.e., >6.5 ‰). The GSB Hadean zircon with the highest $\delta^{18}O$ (SA811p2-186) was measured on three spots with consistent $\delta^{18}O$ values of 8.0 ± 0.3, 8.0 ± 0.3, and 8.3 ± 0.3 ‰ (2s), shows oscillatory zoning (Figure S2 in Supporting Information S1), 92% concordance, and Th/U > 0.1.

Although the $\varepsilon_{Hf(T)}$ and TREE compositions of zircons from the GSB show a significant change at 3.8 Ga, no significant change is observed in the zircon $\delta^{18}O$ signatures. Instead, zircons fall into a similar range of $\delta^{18}O$ values until about 3.5 Ga (Figure 2e). Furthermore, no compositional clustering of zircon ages, $\delta^{18}O$ values, or $\varepsilon_{Hf(T)}$ values occur for any zircons prior to 3.5 Ga (Figure S10 in Supporting Information S1). In contrast, post-3.5 Ga zircons show a more restricted range with stronger clustering in $\delta^{18}O$ values within a given age group. At ~3.4 Ga, the data show a low-$\delta^{18}O$ cluster with 24 zircons showing values ranging from 3.7 ± 0.3 to 4.2 ± 0.3 ‰ (2s). To produce such low $\delta^{18}O$ values, the source material (or major assimilant) must have, at least in part, undergone high-temperature alteration by marine or meteoric waters, such as reported from the Yellowstone volcanic field (Valley et al., 2005). Zircons younger than 3.38 Ga generally plot in the upper mantle field with an average of 5.8 ± 0.7 ‰, but with individual zircons reaching as high as 6.7 ± 0.2 ‰ and as low as 3.7 ± 0.2 ‰ (Figure 2e).

Overall, it is notable that none of the zircon $\delta^{18}O$ values resemble those from Phanerozoic S-type granitoids (Grimes et al., 2011; Valley et al., 2005) and that the range of $\delta^{18}O$ values is similar to what has been previously reported from other Hadean to Archean zircons around the globe (Valley et al., 2005).

4. Discussion

4.1. Crustal Evolution of the Source Terrane to the GSB

Zircons from the GSB reveal a significant shift in the nature of the crust and crustal processes at ~3.8 Ga. The pre-3.8 Ga zircons display consistently negative ε_{HfT} values with a general decrease in ε_{HfT} values from 4.1 to 3.8 Ga. This trend of increasingly negative ε_{HfT} values with time implies that much of the felsic crust in the sources to the oldest GSB zircons was derived from melting or assimilation of a source that originated from a CHUR-like reservoir between 4.4 and 4.2 Ga. The slope of this array may provide an empirical means for determining the average $^{176}Lu/^{177}Hf$ ratio composition of the source of the melts. However, any estimation of a slope will be an oversimplification unlikely to capture the complex history of the crust that sourced the detrital zircons. Early mantle melting likely yielded basaltic crust ($^{176}Lu/^{177}Hf$ value ~ 0.02; Kemp et al., 2010) that may have subsequently undergone partial melting to form more felsic compositions, perhaps TTG-like crust ($^{176}Lu/^{177}Hf$ value ~0.015; Blichert-Toft & Albarède, 2008). Furthermore, the pre-3.8 Ga zircons do not fall on a simple line but rather form a broad band of values, indicative that the zircons were sourced from a range of rock types and/or that the rocks formed over a protracted range of ages. This interpretation is supported by the heterogeneous TREE signature of the zircons, representing the derivation from more mafic to more evolved felsic Hadean crust (Drabon et al., 2021). It is notable that the sources of the >3.8 Ga zircon in the GSB were produced during igneous activity for ~500–600 Ma characterized by intracrustal reworking apparently with little to no addition of felsic crust produced by differentiation from juvenile crust as would be indicated by ε_{HfT} values close to CHUR or above. While it is likely that mantle-derived, juvenile magmatism still occurred prior to 3.8 Ga, these juvenile components were not incorporated into the magmas from which the GSB zircon crystallized.

Based on the trace element signatures of the pre-3.8 Ga GSB zircon, which are similar to those found in ocean islands such as Hawaii or Iceland, much of the initial felsic crust was derived from remelting of mafic crust derived from undepleted mantle sources and reworked in a non-arc setting (Drabon et al., 2021). While this reworking likely included some wet melting, it did not reach full characteristics of subduction-like flux magmatism. The $\delta^{18}O$ data supports that a number of zircons were derived from magmas that assimilated crust that interacted with surface water at low temperatures. Similar to the Jack Hills, there is no correlation between $\delta^{18}O$ and ε_{HfT} for pre-3.8 Ga zircons (Figure S10 in Supporting Information S1). The lack of correlation could reflect the reworking of a diverse assemblage of rocks that previously experienced variable amounts of interaction with liquid water. Together, the ε_{HfT}, TREE and $\delta^{18}O$ data from pre-3.8 Ga zircons are not consistent with melting in a subduction-like setting, which would require relatively radiogenic Hf compositions and TREE evidence that the crust was generated via hydrous melting of a mantle wedge. Instead, the pre-3.8 Ga GSB zircons represent crust that separated from a relatively undepleted mantle during the early Hadean and subsequently remained relatively isolated from the mantle for over 500 Myrs.

Although single analyses of detrital zircons always carry the risk of over-interpretation, the one Hadean zircon (SA811p2-186) that falls significantly below the main ε_{HfT}-time array and exhibits an ε_{HfT} value of -7.0 ± 1.5 (Figure 2b) may indicate early generation of felsic crust. The Hadean age and relatively unradiogenic Hf isotope value requires a relatively low $^{176}Lu/^{177}Hf$, and hence this zircon may have been derived from crust similar in composition to the average modern upper continental crust that formed at ~4.5 Ga (Figure 2b, Array I, $^{176}Lu/^{177}Hf = 0.0125$; Chauvel et al., 2014). The average $\delta^{18}O_{SMOW}$ value of this zircon ($n = 3$) is elevated (+8.1 ‰), requiring that its magmatic source (or a major assimilant) interacted with liquid water at low temperature. This particular grain may have formed from remelting of rocks that initially separated from a CHUR-like mantle reservoir shortly after terrestrial accretion, and that these rocks experienced surface alteration before remelting.

At 3.8 Ga, there is a significant change in the GSB zircon ε_{HfT} and trace element geochemistry. The ε_{HfT} values shift to more radiogenic Hf isotopic compositions. This shift to more radiogenic Hf is consistent with crustal rejuvenation events in which juvenile mantle-derived material was added to the crust and reworked. The moderately subchondritic ε_{HfT} values <3.8 Ga indicate that some older crust continued to be reworked, but this curst either was not older than 3.9-4.0 Ga or it comprised a mixture of juvenile and Hadean crust. Coinciding with

this crustal rejuvenation event, there is essentially no longer isotopic evidence for the continued reworking of 4.3–4.4 Ga protocrust after 3.8 Ga. These observations imply that the previous long-lived Hadean crust was no longer the dominant crustal component and was at best playing only a minor role in the formation of new crust. Concurrent with the shift to higher ε_{HfT} values, the range of U/Nb and Sc/Yb (Figures 2c and 3) ratios broaden considerably and indicate processes involving both arc-like wet and relatively dry mantle melting between 3.8 and 3.65 Ga. This is consistent with the continued generation of zircon-bearing magmas from relatively undepleted mantle sources contemporaneous with the onset of more efficient reworking of crust in arc-like settings. The co-existence of the two source types may reflect separate magmatic-tectonic domains or the interaction of plume-like or rift magmatism with continental crust. The continuous presence of mantle-like and mildly elevated $\delta^{18}O$ signatures in the zircons suggests that the change in tectonic regime did not cause a significant shift in $\delta^{18}O$ compositions of the magmas, as would be the case if the input of weathered and/or diagenetically altered sediments into the magmatic system substantially increased. In general, mildly elevated $\delta^{18}O$ values might not differ enough to distinguish between zircons formed by volcanic resurfacing and those formed from melting of hydrated oceanic crust in a subduction regime if few sediments were involved in the process (Bauer et al., 2020; Grimes et al., 2011; Valley et al., 2005).

Altogether, GSB detrital zircons appear to record a range of crustal sources involved in the formation of felsic crust starting at 3.8 Ga: juvenile crust generated by arc-like processes, juvenile crust generated by melting of the relatively dry mantle (rift and plume-like) with relatively undepleted signatures, and crust generated by reworking or assimilating older crust younger than 4.0 Ga (with either arc-like or relatively undepleted signatures).

After 3.65 Ga, the zircon trace and REE signatures are consistent with derivation both from the relatively undepleted mantle and from arc-like sources. Zircon U/Nb values <20 become rare and most zircon U/Nb values fall either in the transitional zone between arc and mantle (U/Nb 20–40) or fully within the arc magmatism field (U/Nb > 40; Figure 2c). Sc/Yb values more often show clear magmatic arc signatures, especially at 3.65 and 3.31 Ga, while also continuing to show evidence for non-arc contributions. The ε_{HfT} values indicate more frequent reworking of juvenile crustal additions while continuing to indicate the presence of some older crust, however, isotopic evidence for Hadean crust is almost completely lost. It is notable that after 3.65 Ga the GSB zircons start showing more coherent age and compositional TREE and $\delta^{18}O$ clusters instead of a broad band of compositions. This is perhaps indicative of derivation from more distinct, local crustal sources. In the Hf isotope data, the age clusters at 3.38 and 3.31 Ga are characterized by a range in values that reflect mixing between juvenile and evolved isotopic components that can represent lithospheric mantle and crustal components of varying age and composition in the source (Figure 2b). These results resemble ε_{HfT} trends generated by major modern subduction events at continental margins where hydrated oceanic crust interacts with an overlying complex mantle and crustal wedge (Collins et al., 2011; Jones et al., 2015). The zircons of the 3.31 Ga age cluster show the strongest arc-like magmatic zircon TREE signature, with moderate Nb-depletion and strongly elevated Sc/Yb values (Figures 2c and 3, Figure S9 in Supporting Information S1). The combined ε_{HfT} and trace element signatures of this age cluster most strongly mimic modern-day magmatic arc isotopic and trace element signatures.

In summary, the zircons of the GSB crystallized from a variety of melt types, ranging from more juvenile, mantle-derived melts to relatively evolved, arc-like melts that assimilated high- and low-temperature altered crust. The sources show a progressive change from (1) remelting of a long-lived, relatively isolated protocrust from 4.2 to 3.8 Ga with limited recycling of hydrated sediments and crust, to (2) a transitional period from 3.80 to 3.65 Ga reflecting the onset of crustal reworking and juvenile additions while some remaining Hadean crust was reworked, and, (3) after 3.65 Ga, the establishment of isotopic patterns and trace element compositions showing increasing similarities to that of modern subduction zones while rift-plume magmatism continued to play a role.

4.2. Evidence for a Global Transition in the Nature of Evolved Crust Production?

The TREE and hafnium isotope geochemistries of a number of Hadean to Paleoarchean zircon suites show notable similarities, raising the possibility of a similar evolutionary history and indicating that tectonic changes in this time period may have been global in nature.

While Turner et al. (2020) found no evidence for a crustal transition in the Jack Hills zircons based on model melt compositions, we use zircon TREE directly in this study to remove uncertainty associated with estimating Kds. The results show that U/Nb values increase across the 3.8 to 3.6 Ga boundary and that arc-like melting

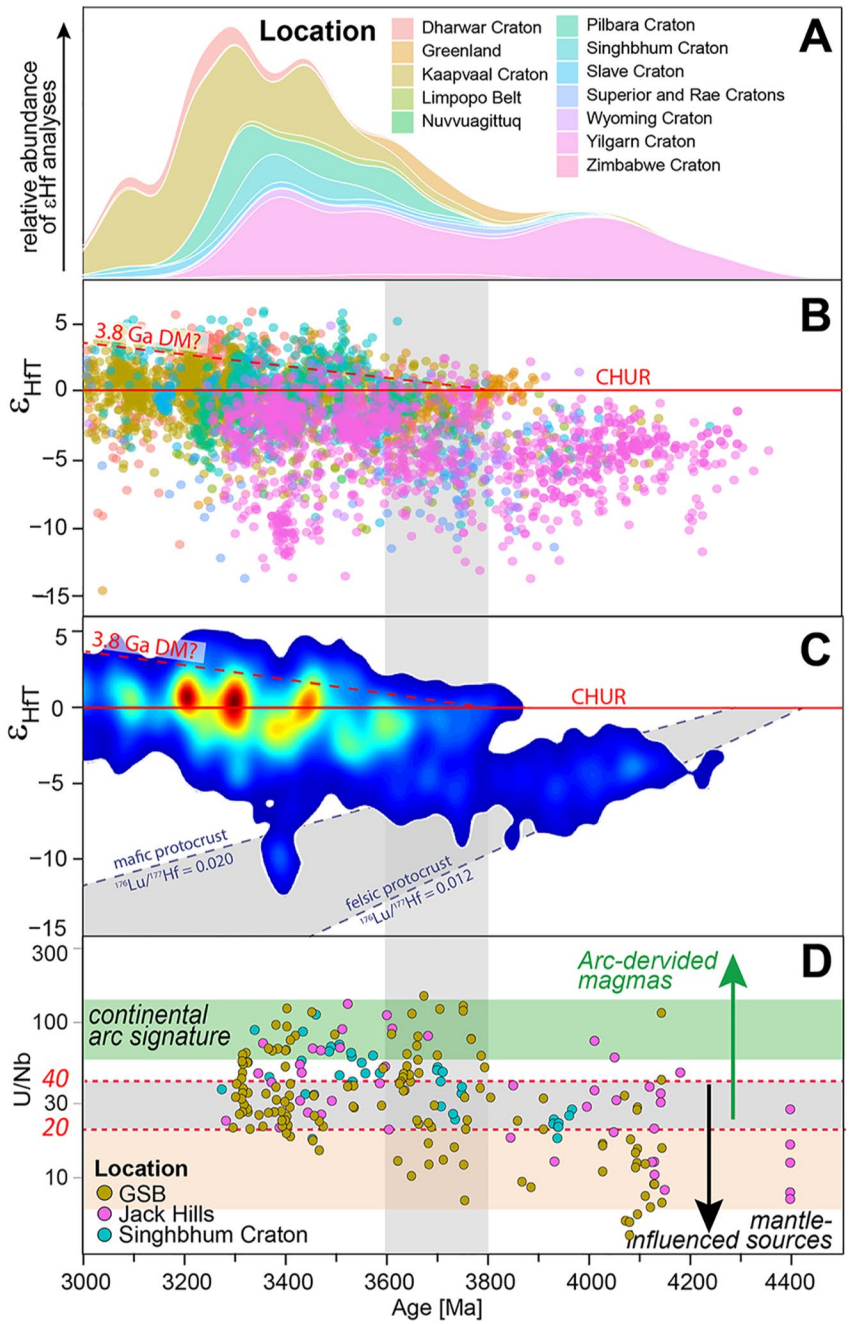

Figure 4. Global compilation of Hadean to Mesoarchean zircons. See Figure S11 in Supporting Information S1 for individual craton evolutions and references. (a) Stacked relative number of Hf isotope analyses for each location through time. Hadean zircons are clearly dominated by those from the Jack Hills in the Yilgarn Craton. (b) Compilation of all zircon Hf isotope analyses for all cratons. Error bars were omitted for clarity. (c) Density plot created using bivariate kernel density estimates (using HafniumPlotter from Sundell et al., 2019). Outer contour represents 95% confidence interval that all other analyses are located within. *Note.* that any global compilation of Hadean zircons is biased toward zircons from the Jack Hills. (d) U/Nb ratios from the GSB, Jack Hills (Peck et al., 2001; Turner et al., 2020), and Singhbhum Craton (Ranjan et al., 2020). The gray vertical bar indicates the proposed transitional period between long-lived protocrust and mobile lid tectonics (e.g., Bauer et al., 2020; Shirey et al., 2008).

signatures become more common after 3.65 Ga (Figure 4d). Jack Hills zircons younger than 3.7 Ga also show higher Sc values (50 ppm) compared to older zircons (17 of 33 analyses below the detection limit of 17 ppm, the remainder averaging 35 ppm; Maas et al., 1992), further supporting a shift to more common arc-like zircon

TREE signatures. Comparable to the GSB zircon suite, these changes in the Jack Hills TREE signature coincide with a shift to ε_{Hf_T} values closer to CHUR. Similarily, zircons from the Singhbhum Craton show an increase in U/Nb values to predominantly arc-like signatures across the 3.8–3.6 Ga transitional period, again concurrently with a shift to more radiogenic Hf isotope values (Ranjan et al., 2020). The difference in U/Nb value of zircons older and younger than 3.8 Ga is statistically significant based on a Welch's t-test ($p = 0.001$). While trace element data from Eoarchean and Hadean zircons are still limited, these results provide support that crust derived from the relatively undepleted mantle in non-arc settings may have played a major role during the early Earth and that arc-like melting conditions became increasingly dominant from 3.8–3.6 Ga. It is noteworthy that at least some whole rock analyses at that time are interpreted to show evidence for flux melting, for example, in Greenland (Jenner et al., 2009; Kamber et al., 2002; Polat et al., 2002).

While samples of Archean and Hadean crust are rare, zircon suites from the Jack Hills, the Singhbhum Craton, the Wyoming Province, the Slave Craton, the Zimbabwe Craton, the Limpopo Belt and now also the Kaapvaal Craton (GSB) show similar subchondritic ε_{Hf_T} values that decrease though time until 3.8 to 3.6 Ga (Bauer et al., 2017; Bell et al., 2011, 2014; Chaudhuri et al., 2018; Kamber, 2007; Kemp et al., 2010; Mueller & Wooden, 2012; Ranjan et al., 2020; Zeh et al., 2014), supporting the notion that the early crust was dominated by long-lived protocrust (e.g., Kemp et al., 2010). While the exact nature of this long-lived protocrust and the crustal processes in operation are still poorly defined, it appears that they were vastly different from those of today. Based on the results presented here, at least some of that early protocrust was derived from the relatively undepleted mantle. The protocrust then experienced internal remelting, some of which involved hydrated crust, but otherwise remained stable for several hundred million years. This isolation of the Hadean crust stands in stark contrast to Phanerozoic oceanic crust, which is typically recycled after <200 Myrs. It is notable that the extraction of the early crust from the chondritic mantle was not a singular global event, which is demonstrated by variation in the timing of CHUR-like ε_{Hf_T} compositions of the Paleoarchean to Hadean zircon suites from different terranes (Figures 4b and S11 in Supporting Information S1). While more data are necessary, this would suggest that if the formation and reworking of a long-lived protocrust, perhaps some form of a stagnant lid, was a dominant process in the formation of evolved crust, then it was a protracted rather than simultaneous process.

Between ~3.8 and 3.6 Ga, a global shift in ε_{Hf_T} values of zircons tracks an increasing contribution from more juvenile source components for the parental magmas (Bauer et al., 2017, 2020; Bell et al., 2011; Chaudhuri et al., 2018; Kemp et al., 2010; Mueller & Wooden, 2012; Ranjan et al., 2020; Figures 4b and 4c, Figure S11 in Supporting Information S1). A global compilation of 3400 igneous and detrital zircons shows a string of high-density, approximately chondritic ε_{Hf_T} clusters starting at 3.8 Ga while isotopic evidence for a long-lived Hadean crustal source becomes rare. After 3.6 Ga, only the Jack Hills zircons show a cluster at 3.38 Ga with unradiogenic Hf that may have formed through reworking of mafic Hadean crust (Figures 4b and 4c). However, Bell et al. (2014) suggested that this negative ε_{Hf_T} cluster does not reflect remelting of Hadean mafic crust but rather of Paleoarchean crust that followed an intermediate $^{176}Lu/^{177}Hf$ trajectory. Not only does the almost complete lack of direct isotopic remnants of Hadean crust after 3.6 Ga imply that the Earth's crust was no longer dominated by long-lived Hadean crust, but that it had become relatively dynamic, where crust was continuously recycled and isotopic remnants of Hadean crust were largely diluted or lost. This transition was a diachronous process and there would have been some period of overlap between tectonic styles. Additionally, after this transition, some of the zircons from the global compilation record superchondritic ε_{Hf_T} values, providing the first evidence for a long-lived, global signature of a depleted mantle, perhaps related to the more efficient formation of continental crust through mobile-lid tectonic processes (represented by the 3.8 Ga depleted mantle line in Figures 4b and 4c; Fisher & Vervoort, 2018; Vervoort et al., 2017).

While ε_{Hf_T} and trace element signatures of pre-3.8 Ga zircon assemblages worldwide are remarkably different from zircons formed in modern plate boundary settings, zircons <3.8 Ga show increasing similarities to modern zircons. In modern subduction settings, the initiation of subduction progressively removes ancient lower crust and the subcontinental lithospheric mantle, initially causing the remelting of older crust with more negative ε_{Hf_T} values (Collins et al., 2011). Following the removal of ancient lower crust, the continuous juvenile additions during mantle wedge melting result in a long-term positive ε_{Hf_T} signature recorded in arc magmas (Collins et al., 2011). Simultaneously, flux melting in subduction zones causes characteristic Nb depletion and Sc enrichment. Plate tectonic processes would likely also be efficient enough in reworking oceanic-type crust, which could account for the almost complete loss of isotopic evidence for the Hadean protocrust. Whether the linked

appearance of these zircon ε_{Hf} and TREE signatures represent the onset of perhaps sluggish plate tectonics or some other mobile-lid process that mimics arc-like melting conditions, such as drip-and-plume tectonics, it provides tantalizing support for a major crustal transition between 3.8 and 3.6 Ga.

5. Conclusions

Detrital zircons from one of the best preserved Hadean to Paleoarchean zircon locations, the GSB, record substantial differences between the crust that formed before and after ~3.8 Ga. Before 3.8 Ga, the longevity of the crust, the absence of juvenile additions to zircon-bearing magmas, and the rarity of evidence for arc-like flux melting conditions are inconsistent with modern style subduction processes. Starting at 3.8 Ga, evidence for pervasive juvenile additions and flux melting becomes increasingly common. A transition similar to that seen in the GSB zircons for TREE and hafnium isotopes occurs in other Hadean-Paleoarchean zircon suites and suggests that the nature of Earth's early crustal processes may have changed permanently between 3.8 and 3.6 Ga. Based on the data presented here, it appears that long-lived protocrust formed in the Hadean and was destabilized, perhaps by the diachronous onset of at least sluggish mobile-lid tectonics, globally starting no later than ~3.8 Ga.

Conflict of Interest

The authors declare no conflicts of interest relevant to this study.

Data Availability Statement

The data is available in Data Sets S1–S10 in the Supporting Information S1 and in the Zenodo database (https://doi.org/10.5281/zenodo.5973863) per AGU's data and software sharing guidance before publication.

Acknowledgments
We thank Sappi and the Mpumalanga Tourism and Parks Agency for access to lands. Funding for travel expenses and analytical costs were kindly provided by the Stanford School of Earth, Energy, and Environmental Sciences at SU and the Earth and Planetary Sciences Department at Harvard University. N. Drabon was financially supported through the Liebermann Fellowship from SU and by the Earth and Planetary Sciences Department at Harvard University. We also thank Emily Stoll, Anton Drabon, William Thompson-Butler, and Jake Harrington for help during sampling. At the USGS Menlo Park, Ruth Dawn's and David Damby's help during the acquisition of CL images was greatly appreciated. The staff of the Arizona LaserChron Center, especially Kurt Sundell, Mark Pecha, and George Gehrels, at the University of Arizona and Matthew Coble at the SHRIMP-RG laboratory at SU were very helpful during detrital zircon analyses. Frédéric Couffignal provided key analytical support in the Potsdam SIMS lab. WiscSIMS is supported by NSF (EAR-2004618) and UW-Madison. JWV and KK are supported by the ERC (Synergy Grant 856555).

References

Baier, J., Audétat, A., & Keppler, H. (2008). The origin of the negative niobium tantalum anomaly in subduction zone magmas. *Earth and Planetary Science Letters*, *267*, 290–300. https://doi.org/10.1016/j.epsl.2007.11.032

Barth, A. P., Tani, K., Meffre, S., Wooden, J. L., Coble, M. A., Arculus, R. J., et al. (2017). Generation of silicic melts in the early Izu-Bonin Arc recorded by detrital zircons in proximal arc volcaniclastic rocks from the Philippine Sea. *Geochemistry, Geophysics, Geosystems*. https://doi.org/10.1002/2017GC006948

Barth, A. P., Wooden, J. L., Riggs, N. R., Walker, J. D., Tani, K., Penniston-Dorland, S. C., et al. (2018). Marine volcaniclastic record of early arc evolution in the eastern Ritter Range pendant, central sierra Nevada, California. *Geochemistry, Geophysics, Geosystems*. https://doi.org/10.1029/2018GC007456

Bauer, A. M., Fisher, C. M., Vervoort, J. D., & Bowring, S. A. (2017). Coupled zircon Lu–Hf and U–Pb isotopic analyses of the oldest terrestrial crust, the >4.03 Ga Acasta Gneiss Complex. *Earth and Planetary Science Letters*, *458*, 37–48. https://doi.org/10.1016/J.EPSL.2016.10.036

Bauer, A. M., Reimink, J. R., Chacko, T., Foley, B. J., Shirey, S. B., & Pearson, D. G. (2020). Hafnium isotopes in zircons document the gradual onset of mobile-lid tectonics. *Geochemical Perspectives Letters*. https://doi.org/10.7185/geochemlet.2015

Bell, E. A., Boehnke, P., Hopkins-Wielicki, M. D., & Harrison, T. M. (2015). Distinguishing primary and secondary inclusion assemblages in Jack Hills zircons. *Lithos*. https://doi.org/10.1016/j.lithos.2015.07.014

Bell, E. A., Harrison, T. M., Kohl, I. E., & Young, E. D. (2014). Eoarchean crustal evolution of the Jack Hills zircon source and loss of Hadean crust. *Geochimica et Cosmochimica Acta*. https://doi.org/10.1016/j.gca.2014.09.028

Bell, E. A., Harrison, T. M., McCulloch, M. T., & Young, E. D. (2011). Early Archean crustal evolution of the Jack Hills Zircon source terrane inferred from Lu-Hf,207Pb/206Pb, and δ18O systematics of Jack Hills zircons. *Geochimica et Cosmochimica Acta*. https://doi.org/10.1016/j.gca.2011.06.007

Blichert-Toft, J., & Albarède, F. (2008). Hafnium isotopes in Jack Hills zircons and the formation of the Hadean crust. *Earth and Planetary Science Letters*. https://doi.org/10.1016/j.epsl.2007.10.054

Blundy, J., & Wood, B. (2003). Partitioning of trace elements between crystals and melts. *Earth and Planetary Science Letters*. https://doi.org/10.1016/S0012-821X(03)00129-8

Bouvier, A., Vervoort, J. D., & Patchett, P. J. (2008). The Lu-Hf and Sm-Nd isotopic composition of CHUR: Constraints from unequilibrated chondrites and implications for the bulk composition of terrestrial planets. *Earth and Planetary Science Letters*, *273*(1–2), 48–57. https://doi.org/10.1016/j.epsl.2008.06.010

Byerly, B. L., Lowe, D. R., Drabon, N., Coble, M. A., Burns, D. H., & Byerly, G. R. (2018). Hadean zircon from a 3.3 Ga sandstone, Barberton greenstone belt, South Africa. *Geology*, *46*(11), 967–970. https://doi.org/10.1130/G45276.1

Campbell, I. H., & Griffiths, R. W. (1993). The evolution of the mantle's chemical structure. *Lithos*, *30*(3–4), 389–399. https://doi.org/10.1016/0024-4937(93)90047-G

Carley, T., Bell, E. A., Miller, C. F., Claiborne, L. L., & Harrison, T. M. (2018). *Striking similarities and subtle differences across the Hadean-Archean boundary: Model melt insight into the early Earth using New Zircon/Melt Kds* (Vol. 2018, pp. V34C–V03). American Geophysical Union, Fall Meeting. *Abstract #*.

Cavosie, A. J., Kita, N. T., & Valley, J. W. (2009). Primitive oxygen-isotope ratio recorded in magmatic zircon from the Mid-Atlantic Ridge. *American Mineralogist*, *94*(7), 926–934. https://doi.org/10.2138/am.2009.2982

Cavosie, A. J., Valley, J. W., & Wilde, S. A. (2005). Magmatic δ18O in 4400-3900 Ma detrital zircons: A record of the alteration and recycling of crust in the Early Archean. *Earth and Planetary Science Letters*, *235*(3–4), 663–681. https://doi.org/10.1016/j.epsl.2005.04.028

Cavosie, A. J., Valley, J. W., & Wilde, S. A. (2019). Chapter 12 - the oldest terrestrial mineral record: Thirty years of Research on Hadean zircon from Jack Hills, Western Australia. In *Earth's oldest rocks* (2nd edn). https://doi.org/10.1016/B978-0-444-63901-1.00012-5

Chaudhuri, T., Wan, Y., Mazumder, R., Ma, M., & Liu, D. (2018). Evidence of enriched, hadean mantle reservoir from 4.2-4.0 Ga zircon xenocrysts from Paleoarchean TTGs of the Singhbhum Craton, Eastern India. *Scientific Reports*, *8*(1), 1–12. https://doi.org/10.1038/s41598-018-25494-6

Chauvel, C., Garçon, M., Bureau, S., Besnault, A., Jahn, B. M., & Ding, Z. (2014). Constraints from loess on the Hf-Nd isotopic composition of the upper continental crust. *Earth and Planetary Science Letters*, *388*, 48–58. https://doi.org/10.1016/j.epsl.2013.11.045

Clement, S. W. J., & Compston, W. (1994). Ion probe parameters for very high resolution without loss of sensitivity. *U.S. Geological Survey Circ.*, *1107*, 62.

Coble, M. A., Vazquez, J. A., Barth, A. P., Wooden, J., Burns, D., Kylander-Clark, A., et al. (2018). Trace element characterisation of MAD-559 zircon reference material for ion microprobe analysis. *Geostandards and Geoanalytical Research*, *42*(4), 481–497. https://doi.org/10.1111/ggr.12238

Collins, W. J., Belousova, E. A., Kemp, A. I. S., & Murphy, J. B. (2011). Two contrasting Phanerozoic orogenic systems revealed by hafnium isotope data. *Nature Geoscience*, *4*(5), 333–337. https://doi.org/10.1038/ngeo1127

Coombs, M. L., & Vazquez, J. A. (2014). Cogenetic late Pleistocene rhyolite and cumulate diorites from Augustine Volcano revealed by SIMS 238U-230Th dating of zircon, and implications for silicic magma generation by extraction from mush. *Geochemistry, Geophysics, Geosystems*, *15*(12), 4846–4865. https://doi.org/10.1002/2014GC005589

Drabon, N., Byerly, B. L., Byerly, G. R., Wooden, J. L., Brenhin Keller, C., & Lowe, D. R. (2021). *Heterogeneous Hadean crust with ambient mantle affinity recorded in detrital zircons of the Green Sandstone Bed, South Africa*. Proceedings of the National Academy of Sciences of the United States of America. https://doi.org/10.1073/pnas.2004370118

Fisher, C. M., & Vervoort, J. D. (2018). Using the magmatic record to constrain the growth of continental crust—The Eoarchean zircon Hf record of Greenland. *Earth and Planetary Science Letters*, *488*, 79–91. https://doi.org/10.1016/j.epsl.2018.01.031

Fisher, C. M., Vervoort, J. D., & Hanchar, J. M. (2014). Guidelines for reporting zircon Hf isotopic data by LA-MC-ICPMS and potential pitfalls in the interpretation of these data. *Chemical Geology*, *363*, 125–133. https://doi.org/10.1016/j.chemgeo.2013.10.019

Fu, B., Page, F. Z., Cavosie, A. J., Fournelle, J., Kita, N. T., Lackey, J. S., et al. (2008). Ti-in-zircon thermometry: Applications and limitations. *Contributions to Mineralogy and Petrology*, *156*(2), 197–215. https://doi.org/10.1007/s00410-008-0281-5

Fu, R. R., Drabon, N., Wiedenbeck, M., Brenner, A. R., Lowe, D. R., & Borlina, C. S. (2021). Paleomagnetism of 3.5-4.0 Ga zircons from the Barberton greenstone belt, South Africa. *Earth and Planetary Science Letters*, *567*, 116999. https://doi.org/10.1016/j.epsl.2021.116999

Gehrels, G., & Pecha, M. (2014). Detrital zircon U-Pb geochronology and Hf isotope geochemistry of Paleozoic and Triassic passive margin strata of Western North America. *Geosphere*, *10*(1), 49–65. https://doi.org/10.1130/GES00889.1

Grimes, C. B., Ushikubo, T., John, B. E., & Valley, J. W. (2011). Uniformly mantle-like δ18O in zircons from oceanic plagiogranites and gabbros. *Contributions to Mineralogy and Petrology*. https://doi.org/10.1007/s00410-010-0519-x

Grimes, C. B., Wooden, J. L., Cheadle, M. J., & John, B. E. (2015). "Fingerprinting" tectono-magmatic provenance using trace elements in igneous zircon. *Contributions to Mineralogy and Petrology*, *170*(5), 1–26. https://doi.org/10.1007/s00410-015-1199-3

Harrison, T. M., Bell, E. A., & Boehnke, P. (2018). Hadean zircon petrochronology. *Reviews in Mineralogy and Geochemistry*. https://doi.org/10.2138/rmg.2017.83.11

Harrison, T. M., Blichert-Toft, J., Müller, W., Albarede, F., Holden, P., & Mojzsis, S. J. (2005). Geochemistry: Heterogeneous hadean hafnium: Evidence of continental crust at 4.4 to 4.5 Ga. *Science*, *310*(5756), 1947–1950. https://doi.org/10.1126/science.1117926

Harrison, T. M., & Schmitt, A. K. (2007). High sensitivity mapping of Ti distributions in Hadean zircons. *Earth and Planetary Science Letters*, *261*(1–2), 9–19https://doi.org/10.1016/j.epsl.2007.05.016

Harrison, T. M., Schmitt, A. K., McCulloch, M. T., & Lovera, O. M. (2008). Early (≥4.5 Ga) formation of terrestrial crust: Lu-Hf, δ18O, and Ti thermometry results for hadean zircons. *Earth and Planetary Science Letters*, *268*(3–4), 476–486. https://doi.org/10.1016/j.epsl.2008.02.011

Hopkins, M., Harrison, T. M., & Manning, C. E. (2008). Low heat flow inferred from >4 Gyr zircons suggests Hadean plate boundary interactions. *Nature*, *456*(7221), 493–496. https://doi.org/10.1038/nature07465

Hoskin, P. W. O., & Black, L. P. (2000). Metamorphic zircon formation by solid-state recrystallization of protolith igneous zircon. *Journal of Metamorphic Geology*, *18*(4), 423–439. https://doi.org/10.1046/j.1525-1314.2000.00266.x

Hoskin, P. W. O., & Schaltegger, U. (2003). The composition of zircon and igneous and metamorphic petrogenesis. *Reviews in Mineralogy and Geochemistry*, *53*(1), 27–62. https://doi.org/10.2113/0530027

Ibanez-Mejia, M., Gehrels, G. E., Ruiz, J., Vervoort, J. D., Eddy, M. E., & Li, C. (2014). Small-volume baddeleyite (ZrO2) U-Pb geochronology and Lu-Hf isotope geochemistry by LA-ICP-MS. Techniques and applications. *Chemical Geology*, *384*, 149–167. https://doi.org/10.1016/j.chemgeo.2014.07.011

Jenner, F. E., Bennett, V. C., Nutman, A. P., Friend, C. R. L., Norman, M. D., & Yaxley, G. (2009). Evidence for subduction at 3.8 Ga: Geochemistry of arc-like metabasalts from the southern edge of the Isua Supracrustal Belt. *Chemical Geology*, *261*(1–2), 83–98. https://doi.org/10.1016/j.chemgeo.2008.09.016

Jones, R. E., Kirstein, L. A., Kasemann, S. A., Dhuime, B., Elliott, T., Litvak, V. D., et al. (2015). Geodynamic controls on the contamination of Cenozoic arc magmas in the southern Central Andes: Insights from the O and Hf isotopic composition of zircon. *Geochimica et Cosmochimica Acta*, *164*, 386–402. https://doi.org/10.1016/j.gca.2015.05.007

Kamber, B. S. (2007). Chapter 2.4 the enigma of the terrestrial protocrust: Evidence for its former existence and the importance of its complete disappearance. *Developments in Precambrian Geology*, *15*, 75–89. https://doi.org/10.1016/S0166-2635(07)15024-6

Kamber, B. S., Collerson, K. D., Moorbath, S., & Whitehouse, M. J. (2003). Inheritance of early Archaean Pb-isotope variability from long-lived Hadean protocrust. *Contributions to Mineralogy and Petrology*, *145*, 25–46. https://doi.org/10.1007/s00410-002-0429-7

Kamber, B. S., Ewart, A., Collerson, K. D., Bruce, M. S., & McDonald, G. D. (2002). Fluid-mobile trace element constraints on the role of slab melting and implications for Archaean crustal growth models. *Contributions to Mineralogy and Petrology*, *144*(1), 38–56. https://doi.org/10.1007/s00410-002-0374-5

Kemp, A. I. S., Wilde, S. A., Hawkesworth, C. J., Coath, C. D., Nemchin, A., Pidgeon, R. T., et al. (2010). Hadean crustal evolution revisited: New constraints from Pb-Hf isotope systematics of the Jack Hills zircons. *Earth and Planetary Science Letters*, *296*(1–2), 45–56. https://doi.org/10.1016/j.epsl.2010.04.043

Kita, N. T., Ushikubo, T., Fu, B., & Valley, J. W. (2009). High precision SIMS oxygen isotope analysis and the effect of sample topography. *Chemical Geology*, *264*(1–4), 43–57. https://doi.org/10.1016/j.chemgeo.2009.02.012

Lowe, D. R., Byerly, G. R., & Heubeck, C. (2012). *Geologic Map of the Barberton Greenstone Bel* (Vol. 103). Geological Society of AmericaMap and Chart Series.

Lowe, D. R., Drabon, N., Byerly, G. R., & Byerly, B. L. (2021). Windblown hadean zircons derived by erosion of impact-generated 3.3 Ga uplifts, Barberton greenstone belt, South Africa. *Precambrian Research*, *356*, 106111. https://doi.org/10.1016/j.precamres.2021.106111

Ludwig, K. R. (2001). *Squid (1.13b), A users manual*. Berkeley Geochronology Center Special Publication.

Maas, R., Kinny, P. D., Williams, I. S., Froude, D. O., & Compston, W. (1992). The Earth's oldest known crust: A geochronological and geochemical study of 3900-4200 Ma old detrital zircons from Mt. Narryer and Jack Hills, Western Australia. *Geochimica et Cosmochimica Acta*, *56*(3), 1281–1300. https://doi.org/10.1016/0016-7037(92)90062-N

Mueller, P. A., & Wooden, J. L. (2012). Trace element and Lu-Hf systematics in Hadean-Archean detrital zircons: Implications for crustal evolution. *The Journal of Geology*, *120*(1), 15–29. https://doi.org/10.1086/662719

O'Neil, J., Boyet, M., Carlson, R. W., & Paquette, J. L. (2013). Half a billion years of reworking of Hadean mafic crust to produce the Nuvvuagittuq Eoarchean felsic crust. *Earth and Planetary Science Letters*, *379*, 13–25. https://doi.org/10.1016/J.EPSL.2013.07.030

Pearce, J. A. (1982). Trace element characteristics of lavas from destructive plate boundaries. In *Andesites: Orogenic andesites and related rocks* (pp. 528–548).

Peck, W. H., Valley, J. W., Wilde, S. A., & Graham, C. M. (2001). Oxygen isotope ratios and rare Earth elements in 3.3 to 4.4 Ga zircons: Ion microprobe evidence for high δ18O continental crust and oceans in the early Archean. *Geochimica et Cosmochimica Acta*, *65*(22), 4215–4229. https://doi.org/10.1016/S0016-7037(01)00711-6

Polat, A., Hofmann, A. W., & Rosing, M. T. (2002). Boninite-like volcanic rocks in the 3.7-3.8 Ga isua greenstone belt, West Greenland: Geochemical evidence for intra-oceanic subduction zone processes in the early Earth. *Chemical Geology*. https://doi.org/10.1016/S0009-2541(01)00363-1

Ranjan, S., Upadhyay, D., Pruseth, K. L., & Nanda, J. K. (2020). Detrital zircon evidence for change in geodynamic regime of continental crust formation 3.7–3.6 billion years ago. *Earth and Planetary Science Letters*, *538*, 116206. https://doi.org/10.1016/j.epsl.2020.116206

Reimink, J. R., Davies, J. H. F. L., Bauer, A. M., & Chacko, T. (2020). A comparison between zircons from the Acasta Gneiss complex and the Jack Hills region. *Earth and Planetary Science Letters*, *531*, 115975. https://doi.org/10.1016/j.epsl.2019.115975

Scherer, E., Münker, C., & Mezger, K. (2001). Calibration of the lutetium-hafnium clock. *Science*, *293*(5530), 683–687. https://doi.org/10.1126/SCIENCE.1061372

Shirey, S. B., Kamber, B. S., Whitehouse, M. J., Mueller, P. A., & Basu, A. R. (2008). A review of the isotopic and trace element evidence for mantle and crustal processes in the Hadean and Archean: Implications for the onset of plate tectonic subduction. *When did plate tectonics begin on planet Earth? 440*, 1–29. https://doi.org/10.1130/2008.2440(01)

Söderlund, U., Patchett, P. J., Vervoort, J. D., & Isachsen, C. E. (2004). The 176Lu decay constant determined by Lu–Hf and U–Pb isotope systematics of Precambrian mafic intrusions. *Earth and Planetary Science Letters*, *219*(3–4), 311–324. https://doi.org/10.1016/S0012-821X(04)00012-3

Sundell, K., Saylor, J. E., & Pecha, M., (2019). Provenance and recycling of detrital zircons from Cenozoic Altiplano strata and the crustal evolution of Western South America from combined U-Pb and Lu-Hf isotopic analysis. In *Andean tectonics* (pp. 363–397). Elsevier. https://doi.org/10.1016/b978-0-12-816009-1.00014-9

Tang, D. L. K., Wilson, C. J. N., Sewell, R. J., Seward, D., Chan, L. S., Ireland, T. R., & Wooden, J. L. (2017). Tracking the evolution of Late Mesozoic arc-related magmatic systems in Hong Kong using in-situ U-Pb dating and trace element analyses in zircon. *American Mineralogist*, *102*(11), 2190–2219. https://doi.org/10.2138/am-2017-6071

Tice, M. M., Bostick, B. C., & Lowe, D. R. (2004). Thermal history of the 3.5–3.2 Ga Onverwacht and Fig Tree Groups, Barberton greenstone belt, South Africa, inferred by Raman microspectroscopy of carbonaceous material. *Geology*, *32*(1), 37. https://doi.org/10.1130/G19915.1

Trail, D., Tailby, N., Wang, Y., Mark Harrison, T., & Boehnke, P. (2017). Aluminum in zircon as evidence for peraluminous and metaluminous melts from the Hadean to present. *Geochemistry, Geophysics, Geosystems*, *18*(4), 1580–1593. https://doi.org/10.1002/2016GC006794

Turner, S., Wilde, S., Wörner, G., Schaefer, B., & Lai, Y. J. (2020). An andesitic source for Jack Hills zircon supports onset of plate tectonics in the Hadean. *Nature Communications*, *11*(1), 1–5. https://doi.org/10.1038/s41467-020-14857-1

Valley, J. W. (2003). Oxygen isotopes in zircon. *Reviews in Mineralogy and Geochemistry*. https://doi.org/10.2113/0530343

Valley, J. W., Kinny, P. D., Schulze, D. J., & Spicuzza, M. J. (1998). Zircon megacrysts from kimberlite: Oxygen isotope variability among mantle melts. *Contributions to Mineralogy and Petrology*, *133*(1), 1–11. https://doi.org/10.1007/s004100050432

Valley, J. W., & Kita, N. T. (2009). In situ oxygen isotope geochemistry by ion microprobe. *Secondary ion mass spectrometry in the earth Sciences*. *Mineralogical Association of Canada*. *Short Courses 41*.

Valley, J. W., Lackey, J. S., Cavosie, A. J., Clechenko, C. C., Spicuzza, M. J., Basei, M. A. S., et al. (2005). 4.4 billion years of crustal maturation: Oxygen isotope ratios of magmatic zircon. *Contributions to Mineralogy and Petrology*, *150*(6), 561–580. https://doi.org/10.1007/s00410-005-0025-8

Vervoort, J. D., Kemp, A., Fisher, C., & Bauer, A. (2016). *Development of the depleted mantle reservoir and growth of the continental crust begins at ~3.8 Ga*. 35th International Geological Congress.

Vervoort, J. D., Kemp, A. I. S., Fisher, C. M., & Bauer, A. M. (2017). Growth of Earth's earliest crust: The perspective from the depleted mantle. In *Annual V.M. Goldschmidt conference*.

Wang, X. L., Coble, M. A., Valley, J. W., Shu, X. J., Kitajima, K., Spicuzza, M. J., & Sun, T. (2014). Influence of radiation damage on Late Jurassic zircon from southern China: Evidence from in situ measurements of oxygen isotopes, laser Raman, U-Pb ages, and trace elements. *Chemical Geology*. https://doi.org/10.1016/j.chemgeo.2014.09.013

Watson, E. B., & Harrison, T. M. (2005). Zircon thermometer reveals minimum melting conditions on earliest Earth. *Science*, *308*(5723), 841–844. https://doi.org/10.1126/science.1110873

Whitehouse, M. J., Nemchin, A. A., & Pidgeon, R. T. (2017). What can hadean detrital zircon really tell us? A critical evaluation of their geochronology with implications for the interpretation of oxygen and hafnium isotopes. In *Gondwana Research*. Elsevier Inc. https://doi.org/10.1016/j.gr.2017.07.007

Wiedenbeck, M., Hanchar, J. M., Peck, W. H., Sylvester, P., Valley, J. W., Whitehouse, M., et al. (2004). Further characterisation of the 91500 zircon crystal. *Geostandards and Geoanalytical Research*. https://doi.org/10.1111/j.1751-908X.2004.tb01041.x

Zeh, A., Stern, R. A., & Gerdes, A. (2014). The oldest zircons of Africa-Their U-Pb-Hf-O isotope and trace element systematics, and implications for Hadean to Archean crust-mantle evolution. *Precambrian Research*. https://doi.org/10.1016/j.precamres.2013.11.006